Oscillatory reactive dynamics on surfaces: A lattice limit cycle model

A. V. Shabunin,[1,2] F. Baras,[3] and A. Provata[2,*]
[1]*Physics Department, Saratov State University, Astrachanskaya 83, 410071, Russia*
[2]*Institute of Physical Chemistry, National Research Center "Demokritos," 15310 Athens, Greece*
[3]*Center for Non-linear Phenomena and Complex Systems, Université Libre de Bruxelles, CP 231, 1050 Bruxelles, Belgium*
(Received 22 February 2002; published 25 September 2002)

Complex reactive dynamics on low-dimensional lattices is studied using mean-field models and Monte Carlo simulations. A *lattice-compatible* reactive scheme that gives rise to limit cycle behavior is constructed, involving a quadrimolecular reaction step and bimolecular adsorption and desorption steps. The resulting lattice limit cycle model is dissipative and, in the mean-field limit, exhibits sustained oscillations of the species concentrations for a wide range of parameter values. Lattice Monte Carlo simulations of the lattice limit cycle model show locally the emergence of sustained oscillations of the species concentrations. Random fluctuations of the concentrations, clustering between homologous species, and competition between the various clusters/species cause the in-phase oscillations of neighboring sites. Distant regions oscillate out of phase and spatial correlations decay exponentially with the distance. The amplitude and period of the local oscillations depend on the system parameters.

DOI: 10.1103/PhysRevE.66.036219 PACS number(s): 82.40.Bj, 05.70.Ln, 82.20.Wt, 02.50.Ey

I. INTRODUCTION

When reactive processes are taking place on low-dimensional supports, the usual mean-field (MF) description may become questionable in the sense that the MF does not reproduce the observed behavior when the underlying microscopic processes are properly incorporated. This indicates an intricate coupling between the microscopic level and the collective behavior described by the macrovariables. Such deviations from the standard description of chemical kinetics have been detected in low-dimensional regular lattices, fractal aggregates or catalytic surfaces [1], or for diffusion-limited reactions in low dimension [2,3]. The origin of these phenomena is to be found in the spontaneous development of inhomogeneous fluctuations that are enhanced by the restricted geometry of the support.

In the case of irreversible surface reactions, the spatial restrictions due to the support coupled to the nonlinear character of the reactive processes may induce substantial deviations from MF. During the last two decades, numerical models have been proposed to explore the mesoscopic behavior of such systems [4–13] and new experimental results have been obtained [14–18]. Some of these studies are based on the minimal Monte Carlo model describing the catalytic oxidation of CO on Pt that was introduced by Ziff *et al.* in 1986 [4–9]. Along the same lines are simulations with surface restructuring [10,11] and superlattice ordering [9]. Similarly, the NO reduction on Pt has been studied using lattice gas models [12] on substrates with different properties [13]. All these studies predict the appearance of complex local patterns, poisoning transitions, and periodic or chaotic oscillations.

To understand the effects induced by the microscopic dynamics at the macroscopic level, one can study more specifically the role of the reactive dynamics on the global behavior, and consider the limit in which the reactant mobility is neglected. In this case, nontrivial effects of space dimensionality have been detected for various types of nonlinear kinetics, showing important discrepancies from MF predictions [19–22].

The emergence of instabilities seems thus to be highly sensitive to the substrate dimensionality and geometry where the reactive processes take place. In particular, for low-dimensional instabilities questions arise as to the persistence of unstable states and to their coupling with the spontaneous spatial organization induced by the restricted geometry. The aim of this paper is to study the complex behavior associated to the development of a *limit cycle* on lattices. Coupling nonlinear oscillators in space automatically perturbs the phases of the local oscillators. This may give rise to destructive interference effects, resulting in the wiping out of the global oscillatory behavior on a macroscopic scale. This is precisely what has been observed in one-dimensional (1D) spatially extended continuous media, where the desynchronization of the local oscillators may lead to the disappearance of the global oscillations [23,24].

To set up reactive lattice dynamics that exhibit complex phenomena, lattice compatibility conditions need to be addressed. The nonlinear reactive scheme involves at least two active chemical species. The nonequilibrium conditions are typically associated with adsorption and desorption mechanisms. This forces one to consider lattices with empty active sites, mimicking open reactive systems. Concomitantly, a conservation condition between adsorbed particles and free sites has to be fulfilled. The flux between the surface and the surrounding gas yields thus a specific structure of the kinetic equations, which has no analog in the fluid-phase macroscopic formulation. These features require developing specific kinetic models already at the MF level. The mesoscopic description that incorporates the lattice structure is then eas-

*Corresponding author. Email address: aprovata@limnos.chem.demokritos.gr

ily implemented using Monte Carlo simulation techniques [4–9].

Along these lines, two of the present authors have previously introduced a lattice generalization of the Lotka-Volterra model under nonequilibrium conditions. The new model was called the ''lattice Lotka-Volterra'' (LLV) model [25]. The LLV model corresponds to an open reactive system involving bimolecular steps representing reaction, adsorption/influx, and desorption/outflux. Only two active species X_1, X_2, and free sites S participate in this scheme,

$$X_1 + X_2 \xrightarrow{k_1} 2X_2, \tag{1a}$$

$$X_1 + S \xrightarrow{k_2} 2X_1, \tag{1b}$$

$$X_2 + S \xrightarrow{k_3} 2S, \tag{1c}$$

Specifically, the lattice compatibility requirement dictates that particles X_1 and X_2 may undergo the autocatalytic transformation (1a) when they are found in adjacent positions on the lattice. An empty site S may adsorb a particle X_1, provided that there is another X_1 in a neighboring site (1b); while a particle X_2 may desorb leaving an empty site S provided that there is another empty site S in the neighborhood (1c). For the LLV model, the MF description predicts a continuum of periodic oscillations whose frequency is fixed by the initial conditions. The lattice dynamics shows a radically different behavior. Especially, on 1D lattice oscillations are suppressed altogether [25,26]. However, on 2D supports, the system naturally selects a preferred frequency depending on the intrinsic parameters and on the lattice geometry [25,27].

Global and coherent oscillations are frequently observed in catalytic reactions on metallic supports [16–31]. Different mechanisms could be involved in this phenomenon, such as a coupling between the chemical process and a structural transformation of the metallic surface. Here we shall investigate the effects produced by a purely reactive process. We will see that the intrinsic nonlinearities are sufficient to sustain oscillations on a lattice without referring to any extra mechanism. Moreover, this study allows us to investigate if and how the Hopf bifurcation is realized on low-dimensional systems.

To study the development of oscillatory instabilities triggered by lattice dynamics, we introduce in the following section the lattice limit cycle (LLC) model that involves a strong autocatalytic step coupled with adsorption and desorption processes. The phase space of the LLC model is investigated for the parameter ranges where the dissipative periodic motion is exhibited. In Sec. III, Monte Carlo simulations on square lattice are presented. This outlines how the MF behavior is modified when the process is realized on a low-dimensional support. The effects of local fluctuations are also discussed. In Sec. IV, quantitative statistical features of the MC results are presented, such as the frequency of oscillations, clustering, and spatial organization. The main results of this work are summarized in the concluding section and new perspectives are suggested.

II. MODEL AND MEAN-FIELD BEHAVIOR

In the early 80s, Aris and co-workers [32,33] have explored the possibility of obtaining sustained oscillations in surface reactions as resulting from the intrinsic nonlinearities of the reactive processes. They have shown that a bimolecular Langmuir-Hinshelwood surface reaction with two empty sites S in its reaction step ($A_{\mathrm{ads}} + B_{\mathrm{ads}} + 2S \rightarrow 4S + P_{\mathrm{g}}$), nonequilibrium conditions associated with the adsorption steps ($A_{\mathrm{g}} + S \rightleftharpoons A_{\mathrm{ads}}; B_{\mathrm{g}} + S \rightleftharpoons B_{\mathrm{ads}}$), and coverage independent parameters may lead to sustained oscillatory reaction rates. The subscripts ''ads'' and ''g'' denote adsorbed and gaseous phases, respectively. It appears that the two empty sites in the reaction step induce a strong nonlinearity that plays the essential role in the emergence of the oscillations. In this model, the limit cycle is characterized by a small basin of attraction. Because of the smallness of the oscillations amplitude, the oscillatory behavior is very sensitive to any perturbation. In this respect, this model is not a good candidate for a mesoscopic description which includes fluctuations.

In a heterogeneous catalysis the so-called vacancy models have been proposed to describe the oscillations observed in the various reduction reactions of NO on Pt surfaces [16]. These processes are typically associated with the use and production of vacant sites. For instance, in the NO+CO reaction, the dissociation of adsorbed NO_{ads} into N_{ads} and O_{ads} requires the presence of one empty site S [28]. With the formation and subsequent desorption of the gaseous products N_2 and CO_2 three sites are liberated. In this case, the structural transformation of the support is not essential for producing oscillations. In the NO+H_2 reduction, the reactive step involves three active chemical species and one vacant site [30,31]. Thus reaction steps involving both the reactants and the vacant sites are thus representative of some heterogeneous catalytic processes. To arrive to a tractable model (containing a minimal number of representative variables) describing such systems, starting from the full mechanism, a drastic reduction is often adopted. The reaction steps may no longer be elementary but represent rather contractions of several elementary reactive processes which are excepted to be fast or negligible as compared to the others. Moreover they strongly depend on the specific type of surface reaction and on the prevailing experimental conditions.

Here we are interested in the generic reactive mechanisms underlying the onset of oscillatory behavior in a lattice. For this purpose, we construct a minimal model exhibiting robust sustained oscillations that may be exhaustively studied at the MF level and easily implemented on a lattice. This will allow us to analyze the influence of the intrinsic nonlinear behavior and disentangle it from other factors such as diffusion, structural transformation of the substrate or lateral interactions. This will help to clarify how the breakdown of the temporal symmetry induced by the limit cycle is affected by the spatial restrictions of the support.

We consider three different species X_1, X_2, and S undergoing the following reactions:

$$2X_1 + 2X_2 \xrightarrow{k_1} 3X_2 + S, \tag{2a}$$

$$X_1 + S \xrightarrow{k_2} 2X_1, \tag{2b}$$

$$X_2 + S \xrightarrow{k_3} 2S. \tag{2c}$$

This scheme is quite similar to the lattice Lotka-Volterra model, except that the reaction step is quadrimolecular. As already pointed out, this strong nonlinearity plays the driving role in the oscillation mechanism. The constraints arising from the underlying lattice have been incorporated, in order to secure conservation of the total number of sites. One of the species, say S, will eventually represent the empty lattice sites.

The species X_1 and X_2 may undergo the autocatalytic transformation (2a) once on the surface. Specifically, we stipulate that when a configuration of four nearest-neighbor sites contains $2X_1$ and $2X_2$, one X_1 particle is transformed in X_2 and the other one desorbs leaving the corresponding site vacant. The step (2b) represents cooperative adsorption of a particle X_1 on an empty site S, provided that another particle X_1 is found on a neighboring site. Similarly, step (2c) stands for the cooperative desorption of a particle X_2, leaving an empty site S, provided that there is another free site in its immediate vicinity. The resulting scheme describes an open nonlinear reactive system submitted to influx of X_1 and outflux of X_2. The constants k_1, k_2, and k_3 represent the reaction rates.

The rate (or mean-field) equations associated with this scheme read

$$\frac{dx_1}{dt} = -2k_1 x_1^2 x_2^2 + k_2 x_1 s,$$

$$\frac{dx_2}{dt} = k_1 x_1^2 x_2^2 - k_3 x_2 s, \tag{3}$$

$$\frac{ds}{dt} = k_1 x_1^2 x_2^2 - k_2 x_1 s + k_3 x_2 s.$$

The conservation condition $x_1 + x_2 + s = \text{const}$ is automatically satisfied. In the sequel the constant will be chosen equal to one, corresponding to the interpretation of x_1, x_2, and s as fractions of the overall lattice, respectively, occupied by X_1 and X_2 particles or being empty. By eliminating $s(=1-x_1-x_2)$, one obtains the reduced system

$$\frac{dx_1}{dt} = -2k_1 x_1^2 x_2^2 + k_2 x_1 (1 - x_1 - x_2),$$

$$\frac{dx_2}{dt} = k_1 x_1^2 x_2^2 - k_3 x_2 (1 - x_1 - x_2). \tag{4}$$

This reduced system admits four steady state solutions:

$$P_1 = (0;0) \quad \text{(empty lattice)}, \tag{5a}$$

$$P_2 = (0;1) \quad \text{(lattice poisoned by } X_1\text{)}, \tag{5b}$$

$$P_3 = (1;0) \quad \text{(lattice poisoned by } X_2\text{)}, \tag{5c}$$

$$P_4 = \left(\sqrt[3]{\frac{k_3^2}{k_1 k_2}[1+K]} + \sqrt[3]{\frac{k_3^2}{k_1 k_2}[1-K]}; \sqrt[3]{\frac{k_2^2}{8k_1 k_3}[1+K]} + \sqrt[3]{\frac{k_2^2}{8k_1 k_3}[1-K]} \right), \tag{5d}$$

where the constant K is only a function of the three reaction rates:

$$K = \sqrt{\frac{(2k_3 + k_2)^3}{27 k_1 k_2 k_3} + 1}. \tag{6}$$

To investigate the structure of the phase space near the fixed points, we perform a standard linear stability analysis. The Jacobian matrix of the system has the form

$$[J] = \begin{bmatrix} -4k_1 x_1 x_2^2 + k_2(1 - 2x_1 - x_2) & -4k_1 x_1^2 x_2 - k_2 x_1 \\ 2k_1 x_1 x_2^2 + k_3 x_2 & 2k_1 x_1^2 x_2 - k_3(1 - x_1 - 2x_2) \end{bmatrix}, \tag{7}$$

where x_1 and x_2 take their stationary values (5a), (5b), (5c), or (5d).

The phase portrait around the four fixed points has the following shape:

(1) The eigenvalues associated with the first fixed point P_1 are $\lambda_1 = k_2$ and $\lambda_2 = -k_3$. The corresponding eigenvectors are $\boldsymbol{e_1} = (1;0)$ and $\boldsymbol{e_2} = (0;1)$, respectively. P_1 is thus a saddle for all physically acceptable (positive) values of the parameters k_1, k_2, and k_3. The attractive manifold directs along the axis x_2 and the repelling manifold is along the axis x_1 (see Fig. 1).

(2) The eigenvalues associated with the second fixed point P_2 are $\lambda_1 = 0$ and $\lambda_2 = k_3$. The eigenvector corresponding to λ_2 is $\boldsymbol{e} = (0;1)$. The phase portrait in the vicinity of this point has no robust character. There is an unstable manifold along the axis x_2 and there is no stable manifold. Trajectories tend to the fixed point P_2 from the right side, and move away from it from the left side (see Fig. 1). Infinitesimal changes in the system equations shifts the eigenvalue $\lambda_1 = 0$, which can become positive or negative. As a result the phase space portrait is modified near this point, which can become either saddle or unstable node. However, it remains unstable and

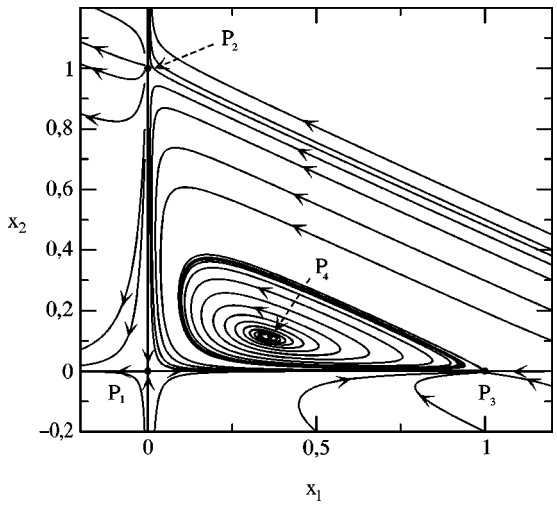

FIG. 1. Phase portrait of the lattice limit cycle model.

the state that corresponds to this fixed point (the species X_2 occupy the whole lattice) cannot be observed.

(3) The eigenvalues associated with the fixed point P_3 has one zero eigenvalue $\lambda_1=0$ and a second eigenvalue $\lambda_2=-k_2$ with corresponding eigenvector $\boldsymbol{e}=(1;0)$. The phase portrait near this fixed point is again not robust. It has a stable manifold along the axis x_1 and has no unstable manifold. Trajectories tend to the point from the bottom ($x_2<0$) and move away from the point from the top ($x_2>0$) (Fig. 1). As for the fixed point P_2 infinitesimal changes of the dynamical scheme can change the phase space portrait near P_3, which can become saddle or stable node. Hence, in such situations where fluctuations drive the system, the state relating to this fixed point (the molecules X_1 occupy the whole lattice) can be observed since it can become stable.

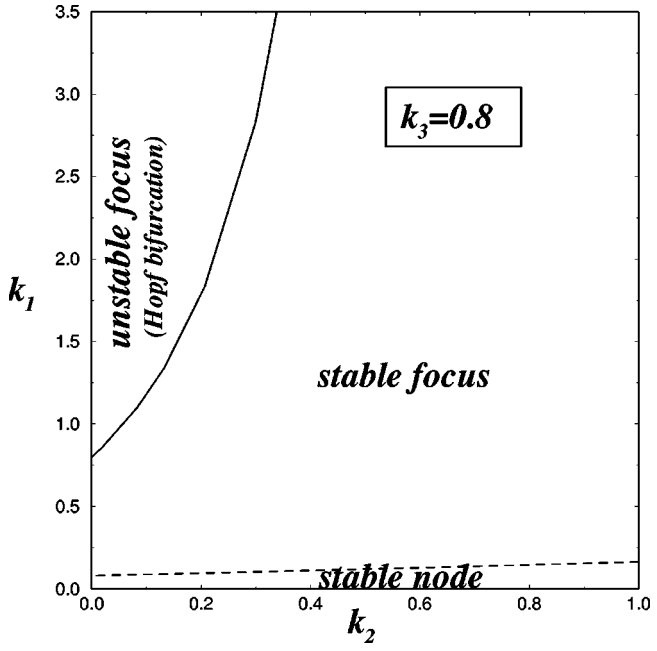

FIG. 2. LLC bifurcation diagram in the parameter space (k_1,k_2) for a constant value of $k_3=0.8$.

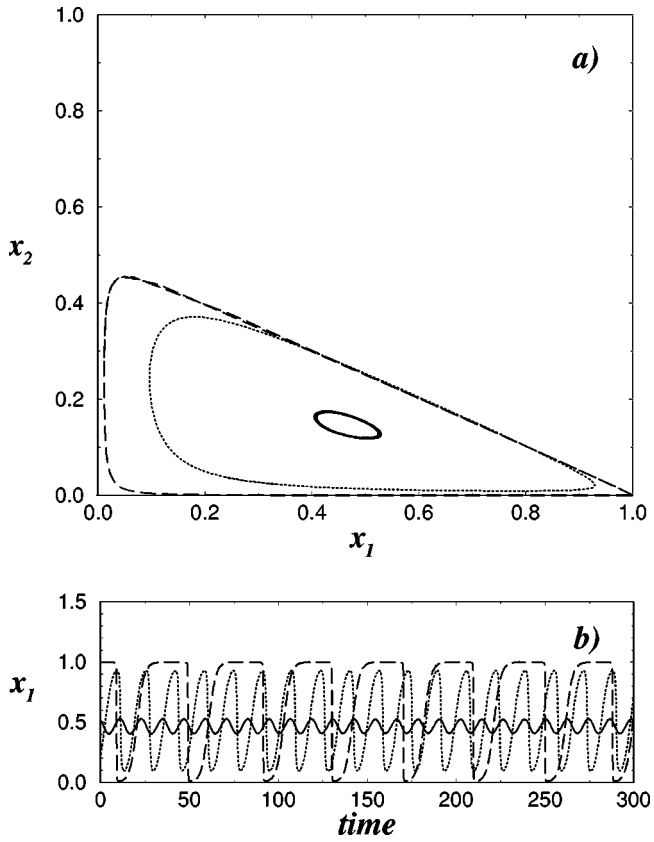

FIG. 3. (a) LLC phase portraits and (b) evolution of the X_1 coverage as a function of time for two different values of the parameter $k_1=10$ (solid line) and $k_1=300$ (dashed lines). The other parameter values remain fixed: $k_2=0.5$ and $k_3=0.8$.

(4) P_4 is a nontrivial fixed point where both X_1 and X_2 species are present on the lattice. Contrary to points P_1,P_2, and P_3, the location of this fixed point and its type depends on the values of the parameters. Depending on the parameters k_1, k_2, and k_3 this point can be: (a) stable node, (b) stable focus, or (c) unstable focus. In Fig. 2, the bifurcation diagram in the parameters plane (k_2,k_1) at fixed value of $k_3=0.8$ is presented. Under the dashed line P_4 is a stable node. On the dashed line both eigenvalues become equal and above the dashed line they are complex conjugate. There the fixed point becomes a stable focus. On the solid line the real parts of these eigenvalues become positive, and the equilibrium undergoes the supercritical Hopf bifurcation. As a result, P_4 becomes an unstable focus and in its vicinity a stable limit cycle appears.

When the focus P_4 loses its stability, periodic oscillations of the concentrations x_1 and x_2 are observed in the system. At the moment of their creation, periodic oscillations have infinitesimal amplitude and their form is harmonic (Fig. 3, solid lines). With gradual parameter changing the amplitude of the oscillations increases and their form becomes nonharmonic. For larger values of the parameter k_1 the amplitude of the oscillations becomes close to 0.5 and the form of the limit cycle is trianglelike (Fig. 3, dashed lines). The behavior of the system is characterized by long residences near the equilibrium P_3 followed by short bursts away from it. From

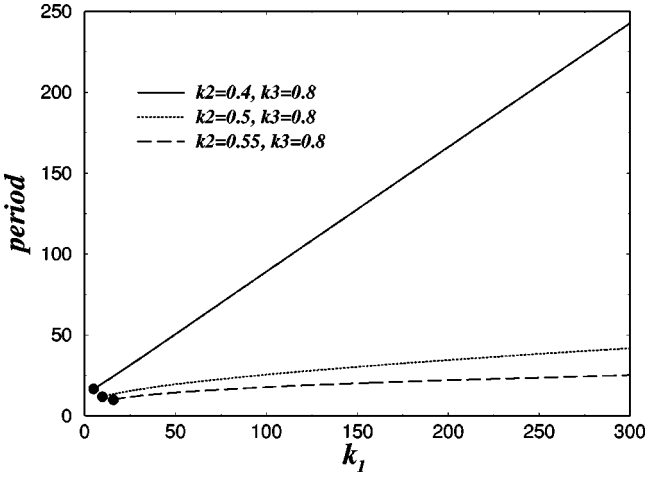

FIG. 4. Oscillation period as a function of the parameter k_1 in the mean-field model for various values of k_2 and k_3.

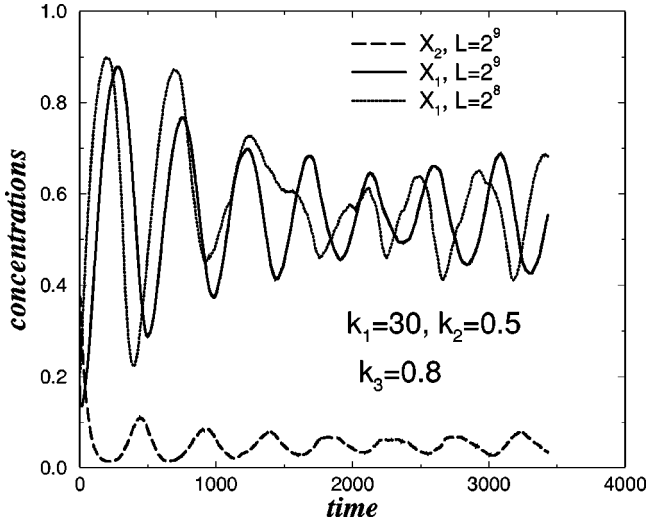

FIG. 5. Temporal evolution of the X_1 (solid line) and X_2 (dashed line) coverages on a two-dimensional square lattice as obtained by Monte Carlo simulations: system size is $2^9\times 2^9$. For comparison the dotted line represents the temporal evolution of X_1 on a smaller system of size $2^8\times 2^8$. Parameter values: $k_1=30$, $k_2=0.5$, and $k_3=0.8$ in all cases.

the reaction point of view the concentration of X_1 stays very close to 1 for a long time, then during the bursts it decreases approximately to zero. In Fig. 4, the dependence of the period of the oscillations on the parameters k_1 is presented. In the same plot the black circles represent the period of small oscillation at the point of appearance of the limit cycle. Unlimited increase of the period is observed, following approximately a linear law.

III. MONTE CARLO LATTICE SIMULATIONS

In the preceding section, we have shown that the LLC scheme produces sustained oscillations at the MF level and seems to be a good candidate for keeping the same behavior when implemented on the lattice. The lattice simulations are designed to emulate the ''microscopic'' picture where each particle reacts locally with a finite number of neighbors on the surface and not with the mean field of all the particles, as implicitly assumed in the usual kinetic description. We assume the existence of a hard core not allowing more than one reacting particle to be at the same lattice node and short range interactions. The mesoscopic approach accounts thus for the random and local nature of the reactive process.

In the limiting case of 1D support, the quadrimolecular step (2a) is not realizable: only the trivial frozen steady state (P_3), corresponding to lattice poisoned by X_1, can be reached. For 2D square lattices, each site has four nearest neighbors and thus all three reaction steps are allowed. The minimum dimensionality of the substrate should thus be equal to 2. In the simulations all the reactants are immobile on the lattice and diffusion effects are not considered.

The Monte Carlo (MC) algorithm on a two-dimensional square lattice is summarized by the following steps:

(i) Initially the lattice is filled at random with particles X_1, X_2 according to a given initial condition. The lattice may also contain empty sites *S*.

(ii) At every elementary MC step, one lattice site is chosen at random.

(iii) If the chosen site is occupied by a particle X_1 and if amongst its four nearest neighbors two particles of type X_2 and one particle of type X_1 are found then reaction (1a) takes place: the chosen site X_1 and its neighbor occupied by X_1 are replaced by an empty site *S* and a particle X_2, respectively, with reaction probability $p_1=k_1/(k_1+k_2+k_3)$. The algorithm then returns to stage (ii) for a new step to start.

(iv) If the chosen site contains an X_2 particle and a randomly chosen neighbor is free, then X_2 desorbs and the site is vacated with probability $p_3=k_3/(k_1+k_2+k_3)$. This is the realization of the desorption process (1c). The algorithm returns to stage (ii).

(v) If the chosen node is empty, *S*, and a randomly chosen neighbor contains an X_1 particle then a second X_1 adsorbs on the *S* site with adsorption probability $p_2=k_2/(k_1+k_2+k_3)$. This is the realization of the adsorption process (1b).

(vi) In all other cases the lattice remains unchanged.

(vii) The algorithm returns to stage (ii) for a new reaction event to start.

The time unit in the MC procedure is defined as the number of elementary MC steps equal to the total number of lattice sites. If the linear size of the system is *L*, then in one MC time unit $(L\times L)$ attempts of reactive events take place.

As working parameter set for the simulations the rate constants $k_1=30$, $k_2=0.5$, and $k_3=0.8$ are chosen for which, at the MF level, the limit cycle presents a reasonably extended basin of attraction as seen in Fig. 5. The reaction probabilities for each step are $p_1=0.9585$, $p_2=0.0160$, and $p_3=0.025\,56$. In the MC simulations the actual reactivity is greatly limited by the environment and the global reactivity rate *A*, defined as $A=$ (number of efficient reactions)/(number of MC steps), is of the order of 0.004 for this choice of parameters. In Fig. 5, the global concentrations of particles X_1 (solid line) and X_2 (dashed line) as a function of time are plotted, for a square lattice of size $2^9\times 2^9$. Sustained oscillations are observed as predicted from the MF

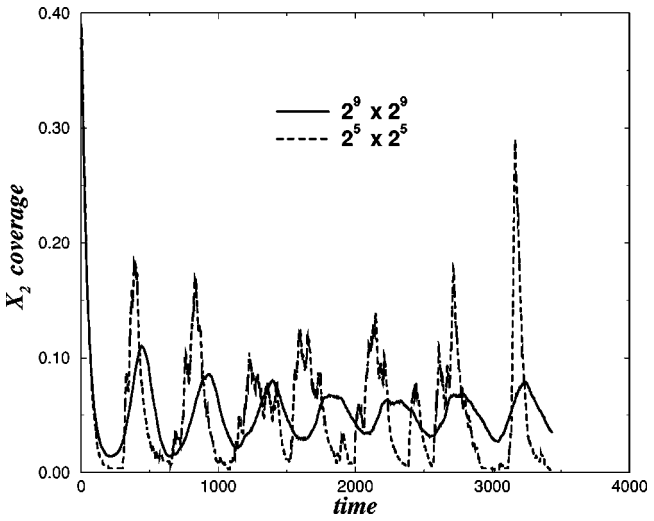

FIG. 6. Temporal evolution of the X_1 and X_2 coverages for a square lattice $2^9 \times 2^9$ (solid line) and for a sublattice $2^5 \times 2^5$ (dashed line). Same parameters as in Fig. 5.

description. These oscillations are robust under a wide choice of initial conditions.

The influence of the system size is illustrated in the same figure with the time dependence of X_1 coverage. The solid line corresponds to a $2^9 \times 2^9$ lattice, while the dotted line corresponds to a $2^8 \times 2^8$ one. Although the system size changes by a factor of 4, the amplitude and frequency of the global oscillations do not vary significantly. To test further the development of the oscillations we focus on the subregions of the original system and record data simultaneously, both for the total system and for the subregion. Comparative results are presented in Fig. 6. The solid line corresponds to the time evolution of the concentration of X_2 on the entire lattice of size $2^9 \times 2^9$ sites, while the dashed line represents the time evolution of X_2 in a small sublattice of size $2^5 \times 2^5$. A difference in the amplitude of oscillations is observed between the subregion (larger amplitude of oscillations) and the entire system (smaller amplitude).

As the system size increases and exceeds a given parameter dependent threshold, (the linear length $L_{th} > 2^{11}$ for the working parameter set), global oscillations are hardly detectable and the system, at first sight, reaches a steady state characterized by constant global concentrations. However, careful examination of subregions of size $l \times l$ ($l < L_{th}$) shows that oscillatory behavior is still highly observable within the system, as was also indicated in Fig. 6. This indicates that locally the system is coherent and small regions/neighborhoods intercommunicate and oscillate inphase. Instead, distant regions are out of phase and when the ensemble on all local oscillators is considered, the local oscillatory behavior is masked.

The development of the local oscillations is directly related to the difference in the time scales of the three processes (2a), (2b), and (2c), and to the autocatalytic character of the chemical scheme. The creation of one X_2 particle requires the presence of two X_2 particles and two X_1 in an immediate neighborhood. This makes the reaction possible only at the borders between X_1 regions and X_2 regions. Under reaction (2a), the X_2 regions propagate through X_1 domains. Once a small X_2 cluster appears, due possibly to local fluctuations, it propagates fast within the X_1 regions because of the relatively large value of the kinetic constant k_1. Concomitantly, from the interior of this growing cluster individual X_2 particles will start desorbing according to Eq. (2c). The desorption process is slower than the growth of the X_2 clusters. Eventually the desorption of internal X_2 particles depletes slowly the cluster interiors. When sufficiently large empty regions are produced, X_1 particles can be deposited. This adsorption process takes place relatively infrequently, due to the autocatalytic nature of the process (2b) and the small value of the kinetic constant k_2. Once the X_1 regions thus produced come into contact with X_2 regions the same oscillatory scenario is repeated.

The different steps of this process are illustrated in the three snapshots of Fig. 7. The black sites and gray sites represent the X_2 and the X_1 particles, respectively. The empty sites are depicted in white. Figure 7(a) corresponds to the beginning of cluster formation. In Fig. 7(b) the clusters are extending. We note that the X_2 particles are distributed at the borders of growing empty surfaces. Figure 7(c) shows that the clusters cover progressively a large extent of the surface, whereupon destruction starts in their interior and X_1 particles start to adsorb forming X_1 clusters.

From the previous discussion it is evident that the size of the oscillatory regions R depends on the competition between the three processes and on their relative rates. The size R can change, grow or shrink, by appropriately changing the relative velocities. Alternatively, the values of k_1, k_2, and k_3 determine the maximum cell size R, within which the particles ''intercommunicate,'' oscillating in phase. If the system size is smaller than or equal to R, the entire system behaves as a single oscillator. The systems of size greater than R contain more than one oscillators and thus negative ''interference'' phenomena take place. In the limit of very large systems of sizes $L > L_{th} > R$, many oscillators with different phases are randomly distributed and their phases are mutually cancelled.

As the value of k_1 increases relatively to k_2 and k_3, the behavior is characterized by abrupt ''bursts'' and slower decays of X_2 (and similarly for X_1 and S). However, this effect is only local, while globally the oscillations are smooth and statistically symmetric. In Fig. 8 the concentrations of X_2 are presented as a function of time for rate constants $k_1 = 300$, $k_2 = 0.5$, and $k_3 = 0.8$. The solid line corresponds to concentration over the entire lattice of size $2^9 \times 2^9$, while the dashed line corresponds to a sublattice of size $2^5 \times 2^5$. While in the entire lattice the oscillations are relatively smooth and symmetric, in the sublattice (dashed line) the oscillations become nonsymmetric: for some time the sublattice concentration of X_2 builds up abruptly, while the concentration of X_1 (not shown) decays slowly, then X_1 spends sometime approaching zero and then suddenly bursts up. This effect is predicted globally by the MF (see Fig. 3, dashed lines). The comparison of the sublattice oscillations (dashed lines) in Figs. 6 and 8 shows that in the former case ($k_1 = 30$) the sublattice oscillations are statistically symmetric, while in the latter ($k_1 = 300$) they have triangular form. This is in

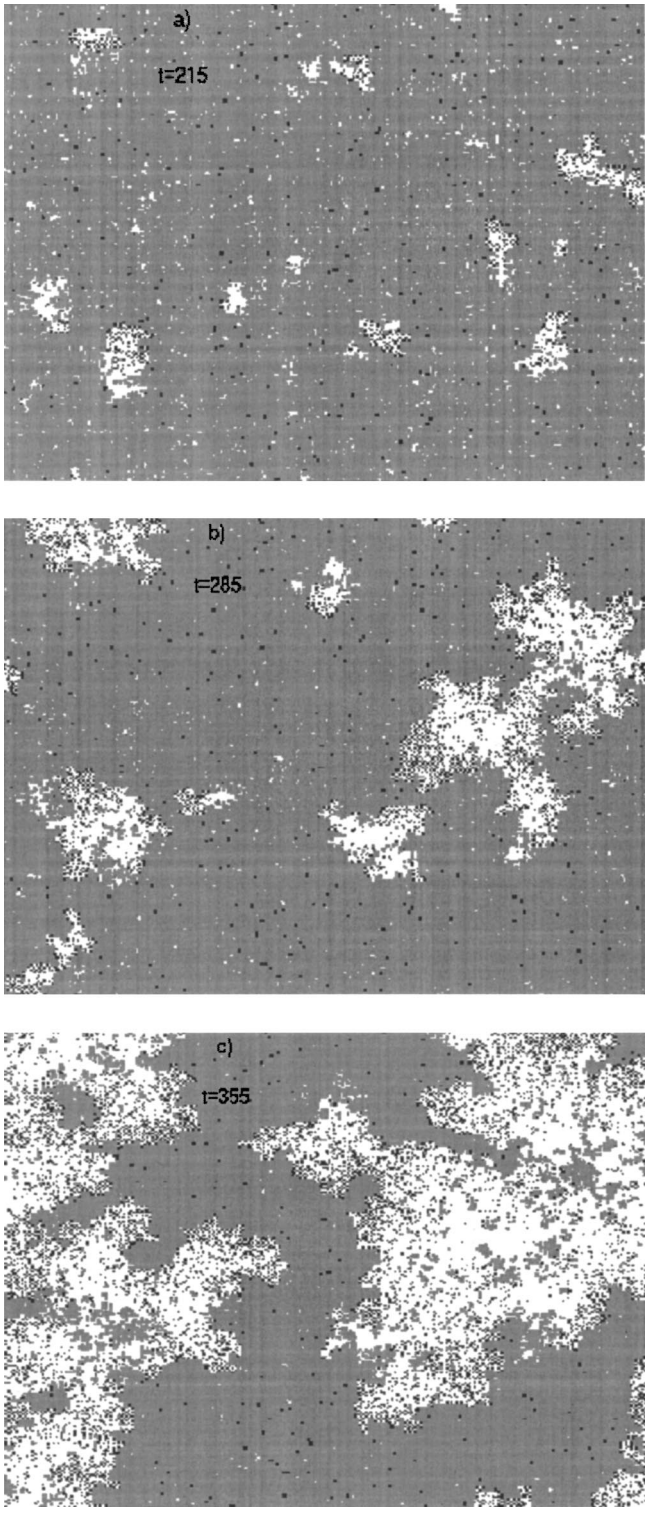

FIG. 7. Three different stages of cluster growth and destruction for a lattice of size $2^8 \times 2^8$. Snapshots (a), (b), and (c) correspond to times $t=215$, 285, and 355 (in MC units), respectively. Same parameters as in Fig. 5.

agreement with the MF results (Fig. 3, dashed lines) indicating that as k_1 increases the form of the oscillations changes gradually from the symmetric, nearly harmonic shape towards the triangular form. Finally, when the relative velocities k_i's become of the same order of magnitude, then the regions of ''intercommunication'' shrink and either a simple statistical steady state is reached or even a frozen state is reached.

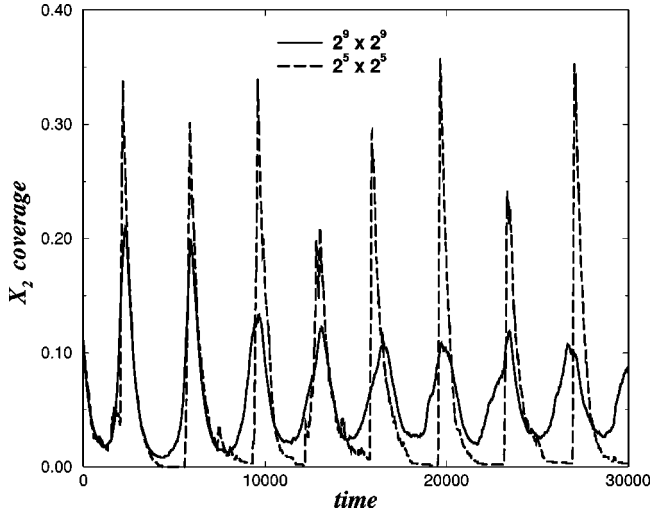

FIG. 8. Temporal evolution of X_2 coverage for parameter values $k_1=300$, $k_2=0.5$, and $k_3=0.8$. On a large lattice $2^9 \times 2^9$ (solid line), smooth oscillatory patterns are observed, while locally, on a sublattice of size $2^5 \times 2^5$, sudden bursts followed by slow decays are observed.

IV. QUANTITATIVE DESCRIPTION

To interpret the spatial organization and temporal coherence revealed in the preceding section, we evaluate the statistical properties of the datasets generated by the MC simulations.

As a useful indicator for clustering we consider the nearest-neighbor covariance $V(t)$ [25],

$$V(t)=\frac{1}{L^d}\sum_{\vec{r}} \sigma_{\vec{r}}(t)\sigma_{\vec{r}+\vec{\epsilon}}(t), \tag{8}$$

where $\vec{r}$ represents a given lattice site (i,j), $\vec{\epsilon}$ is the set of first neighbors of $\vec{r}$, and $\sigma_{\vec{r}}(t)$ denotes the state of site $\vec{r}$ at time t. The variable σ takes the values 0, 1, or -1 whenever the site $\vec{r}$ contains a particle of the type S, X_1, or X_2, respectively.

It is easy to show that for a uniform random distribution with equal mean coverage 1/3, without clustering effects, the nearest-neighbor covariance is, on the average, equal to 0. Indeed, the product $\sigma_{\vec{r}}(t)\sigma_{\vec{r}+\vec{\epsilon}}(t)$ can only take the values 0, 1, or -1. For random lattices the value of σ on site $\vec{r}$ is independent of the value $\vec{r}+\vec{\epsilon}$. Thus the product takes the value 0 with probability 5/9, the value 1 with probability 2/9, and the value -1 with probability 2/9. Consequently, for a large random distribution of X_1, X_2, and S the sum of all the products is equal to zero.

When clustering takes place, most of the sites in a certain neighborhood (cluster) have the same sign, thus the contribution to the sum (8) within clusters is positive. The negative

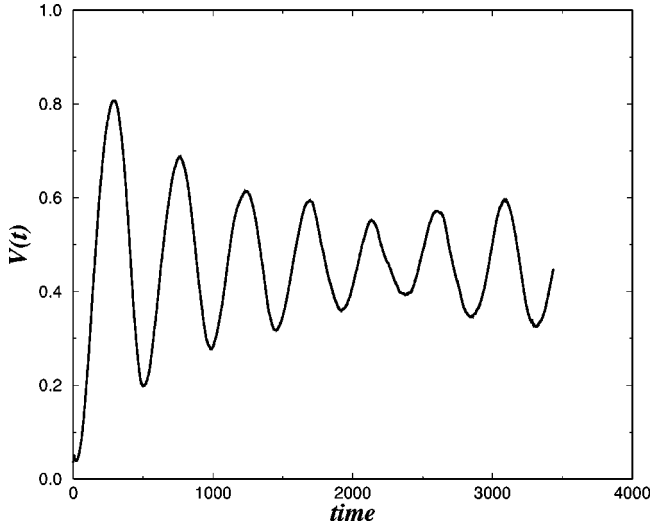

FIG. 9. Evolution of the covariance function $V(t)$ as a function of time. Parameter values as in Fig. 5.

contribution appears only in the interface between X_1 and X_2 clusters. In Fig. 9, the covariance $V(t)$ is presented as a function of time, for a system of size $2^8 \times 2^8$ sites and kinetic constants $k_1=30$, $k_2=0.5$, and $k_3=0.8$. At the beginning of the simulation, one starts with a completely random system and as expected the value of $V(t)$ is close to zero. The initial deviation from the value 0, in Fig. 9 is attributed to random fluctuations. As the time increases the clusters of X_2 form and thus $V(t)$ increases reaching values as high as 0.7. The system passes sequentially from a state of high clustering to a state of low clustering, where the function $V(t)$ takes values as small as 0.2. Note that clusters of empty sites do not contribute to the value of $V(t)$. The overall shape of $V(t)$ presents the same oscillatory characteristics as the fractional coverage. This behavior of $V(t)$ suggests that neighboring particles should oscillate in phase. As we will see shortly (cf. Fig. 11), the correlation length actually covers several layers of neighbors and thus nearest neighbors perform similar motion.

To characterize the temporal coherence within the system, the coarse-grained normalized time-correlation function $C(\tau)$ is considered,

$$C(\tau)=\frac{1}{N}\sum_{t_i=1}^{N}\frac{1}{\langle \delta\zeta_l^2\rangle}[\zeta_l(t_i)-\langle\zeta_l\rangle] \times[\zeta_l(t_i+\tau)-\langle\zeta_l\rangle], \tag{9}$$

where l denotes the set of nodes belonging to a subregion and

$$\zeta_l(t_i)=\sum_{\vec{r}\epsilon l}\sigma_{\vec{r}}(t_i) \tag{10}$$

is the average value of the variable in the coarse-graining region l, $\langle \delta\zeta_l^2\rangle$ is the corresponding variance. The average, in Eq. (9), is taken over N time steps.

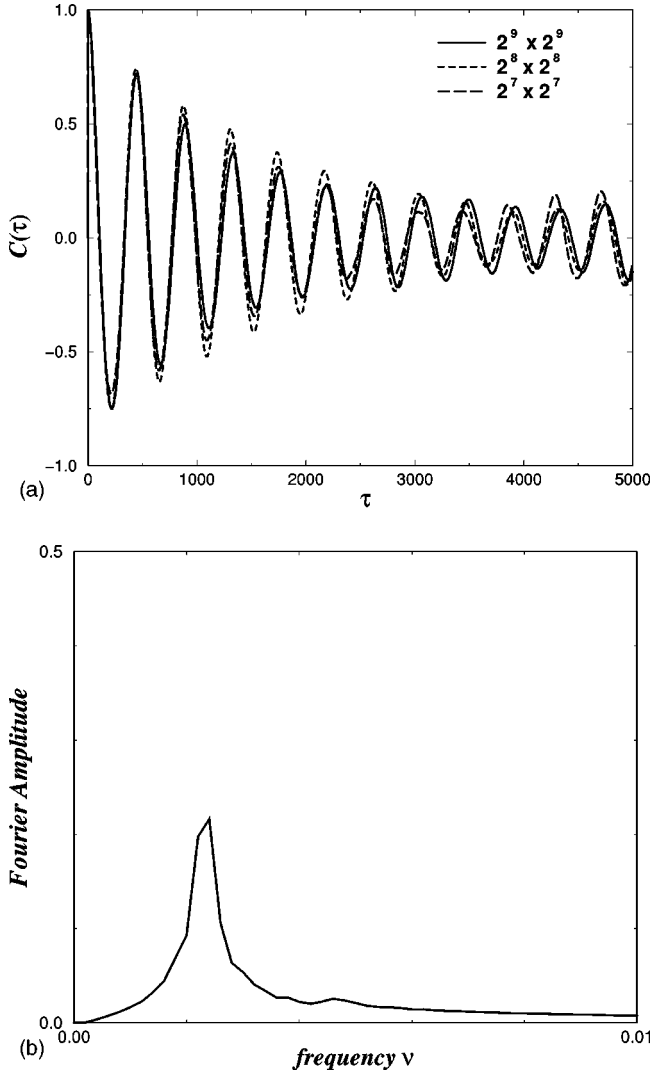

FIG. 10. (a) Normalized time-correlation function of X_2 species computed for the entire lattice and for two sublattices. (b) Corresponding power spectrum for the large system. Same parameters as in Fig. 5.

As we have seen in Fig. 6, the oscillations' amplitude of the coarse-grained variable ζ_l is strongly reduced for a large system as compared to a smaller one. On the other hand, the larger the region, the smaller the variance to the mean, $\langle \delta\zeta_l^2\rangle$, will be. These two effects counterbalance in the expression of $C(\tau)$.

In Fig. 10(a), the time correlation of the X_2 coarse-grained variable is presented for three different values of l: (a) $L \times L=2^9\times 2^9$, which corresponds to the full lattice (solid line); (b) $l_1\times l_1=2^8\times 2^8$, which represents one quarter of the lattice (dotted line); and (c) $l_2\times l_2=2^7\times 2^7$, which is one sixteenth of the lattice (dashed line). The three curves are practically identical, which indicates high temporal coherence for the entire system or in a subregion, at the level of the scaled variable $\zeta_l/\langle \delta\zeta_l^2\rangle^{1/2}$. Figure 10(b) depicts the power spectrum associated to the correlation function $C(\tau)$. The system exhibits a single preferred frequency, independently of the size and in accordance with the MF limit cycle behavior.

TABLE I. Oscillation period (in MC units) and surface activity measured in MC simulations as a function of k_1.

k_1	MC period	q	Activity (Å)
20	470±15		0.0080
25	517±20	9.4	0.0071
30	590±20	14.6	0.0064
35	633±15	8.6	0.0058
40	693±30	12.0	0.0052
45	750±30	11.4	0.0048
50	815±30	13.0	0.0043

To investigate further the correspondence between the MF and its lattice counterpart, we estimate the oscillation period for several values of k_1, keeping the other rate constants equal: The parameters set is chosen for comparison with the solid line of Fig. 4 ($k_3=0.8$ and $k_2=0.4$). As can be seen in Fig. 4, the limit cycle MF period, as obtained by direct integration of Eqs. (3), grows linearly with k_1. The system used in MC simulations has linear size $L=2^{10}$ and its dynamical evolution is recorded over 3×10^4 MC steps, after the system has reached the steady state oscillatory regime. For larger values of k_1, the system size is too small for appearance of the full oscillatory regime. The MC period of the concentration oscillations is obtained by computing the Fourier transform of the time-correlation function. The quantity q accounts for the change in the period P of the MC oscillations, with respect to variations in the reaction rate k_1,

$$q=\frac{P-P'}{k_1-k_1'}. \tag{11}$$

In the MC simulations the values of q have a certain dispersion about 10%, due to the width of the corresponding peaks in the Fourier spectrum. The MC values of q are randomly dispersed around the mean value $\tilde{q}=11.5$ and no general tendency of q is observed with increasing values of k_1. The value $\tilde{q}$ corresponds to a linear increase of P with respect to k_1, which is consistent with the mean-field results.

We have also recorded the surface activity (or reactivity rate) A, which is defined as the number of *reactive events* (i.e., events that have actually changed the lattice configuration) divided by the total number of attempts (i.e., the total number of elementary MC steps). In surface reactions, a reactive attempt will lead to the change of state of a chosen lattice if the local configuration of its neighbors is appropriate. The substrate restrictions imply that the reactivity rate is not only related to the reaction probabilities. On the contrary, in the MF approximation, reactions take place at every time step with a prescribed rate. In the definition we adopted, the reactivity A is a global quantity that accounts for all the elementary reactive events.

In Table I, we observe that the surface activity A is reduced when k_1 is increased. This seems to be in contradiction to what one would expect, since increase of any of the three reaction constants should favor the lattice reactivity. However, as k_1 is getting larger, while k_2 and k_3 remain constant, the size that the X_2 clusters reach becomes rather large before reactive steps (2b) and (2c) come into play. The system is then covered by a few large X_2 clusters and some isolated X_1. Consequently, the length of the boarderlines between clusters where reactions occur is highly reduced. The inefficiency of the reactive process reflected by the low A value is due to the fact that the entire lattice is practically invaded by one species and that the size of the reactive area tends to zero.

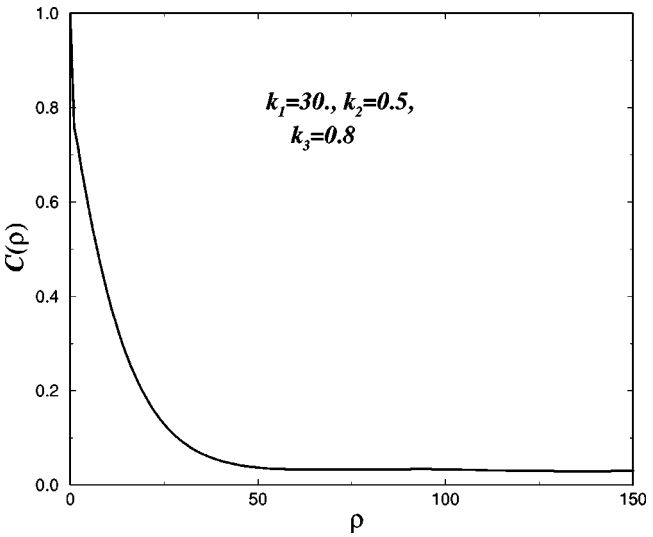

FIG. 11. Spatial-correlation function $C(\rho)$ as a function of ρ for a two-dimensional lattice $2^9\times2^9$ divided into 512 slices. Same parameters as in Fig. 5.

This type of non-MF behavior has already been detected experimentally [18]. Using scanning tunneling microscopy (STM) visualization techniques, Wintterlin *et al.* have found deviations from MF in the CO oxidation on Pt. By recording STM images during the reaction of adsorbed oxygen atoms and CO molecules on a small area of Pt(111) (17 nm × 18 nm) in a pure CO atmosphere, they have observed that the reaction is not taking place randomly but is restricted to the boundaries between O_{ad} and CO_{ad} domains. By measuring the rate of disappearance of adsorbed atomic oxygen, they have concluded that the reaction rate is no more given by the usual MF but is, rather, directly proportional to the length of the boundaries.

To further characterize the spatial coherence in the system, we compute the spatial correlation function that is defined as

$$C(\rho)=\frac{1}{NL^d}\sum_{t_i=1}^{N}\sum_{\vec{r}}\sigma_{\vec{r}}^{X_2}(t_i)\sigma_{\vec{r}+\vec{\rho}}^{X_2}(t_i). \tag{12}$$

The variable $\sigma_{\vec{r}}^{X_2}$ takes the value 1 or 0, accordingly, as the lattice site $\vec{r}$ contains a X_2 particle or not. To evaluate this function, it is useful to adopt a coarse-grained description in which the lattice is divided along one direction in l slices. The correlation function is then evaluated for the global σ variable along the chosen direction. Owing to the averaging within each slice one obtains, in this way, a smooth behavior.

Figure 11 depicts the results of the numerical evaluation

of Eq. (12) for a $2^9 \times 2^9$ lattice divided in 512 slices. Average is taken over $N = 5 \times 10^4$ MC time steps. One observes a decrease, which turns out to be exponential, with a characteristic correlation length of about 15 lattice sites. This further confirm the persistence of large clusters of homologous particles. It also fixes the mean intrinsic size of such clusters all along the reactive process.

V. CONCLUSIONS AND PERSPECTIVES

It is now well known that, in many situations, the local surface constraints lead to deviations from the usual mean-field description. While typical instabilities such as those leading to transitions to multiple states are fairly well understood from this standpoint, the case of symmetry-breaking transitions such as those leading to limit cycle remains intriguing. It is important to understand how the nonlinear dynamics that tends to break down the temporal symmetry in the bulk is affected by the spatial restrictions. In order to understand these aspects, mesoscopic Monte Carlo simulations and the macroscopic MF approach need to be compared in detail.

We constructed a minimal model that is tractable at the MF level and may be directly implemented in the lattice simulations. This allows to study the *generic aspects* of complex dynamical behavior associated with the limit cycle. In our work, the incidence of the kinetics is thus studied independently of other factors whose influence will be considered in subsequent investigations. This representative model is not related to a specific surface reaction, but contains the necessary complexity to generate the desired phenomenon.

The LLC model describes an open reactive system under nonequilibrium conditions. The reactive scheme involves adsorption, desorption, and reaction steps, under the condition that the total number of on-lattice interacting particles plus the empty lattice sites be conserved throughout the process. In the MF description LLC is a dissipative system. For a large range of parameter values all the phase space trajectories sink into a limit cycle; the MF concentrations oscillate in time with constant amplitude. The amplitude and the period of the oscillations depend only on the various system parameters.

When the LLC model is realized on a lattice, the picture changes radically. On square lattice (2D), clustering of homologous particles is observed and local oscillations appear. The lattice is divided into subregions that oscillate in phase, while distant oscillating subregions are out of phase. Consequently, for large enough systems, the local oscillators are active while the global oscillations are suppressed. The development of the local oscillations is attributed to excitations of random lattice sites due to local fluctuations. These excitations propagate with rates depending on the system parameters and on the lattice characteristics.

From preliminary investigations, the frequency and amplitude of the local oscillations depend not only on the parameters of the system but seem to depend strongly on the local properties of the lattice (average number and distribution of nearest neighbor sites). A first extension of the present work would be the realization of the reaction scheme on hexagonal lattice, where the immediate neighborhood contains exactly four sites, the same exact number of sites required for the multiparticle reaction step (2a). Also, of interest would be the LLC realization on a lattice with locally variable number of nearest neighbors. The coupling between the dynamics generated by a minimal model such as the LLC with transitions between lattice geometries would also be worth investigating, since in some experimental situations, transformations between different support geometries are observed [16].

A second direction extending the present work would be to investigate the role played by diffusion and its interference with the oscillatory behavior. Two opposite situations could happen. Diffusion could lead to the homogenization of the reactants distributions or, on the contrary, favor the spontaneous clustering of homologous particles. A deep understanding of transport processes on restricted supports requires careful modeling of diffusion at the microscopic level. In some cases, the mobility of the reactants may be modeled as an activated process associated with the jump of particles from on site to one of its nearest neighbors. In other situations, all the particles belonging to a surface ''bath'' could move synchronously.

Our results confirm further the idea that the support may modify the MF behavior both statically and dynamically. Representative low-dimensional models, which exhibit complex phenomena at the MF level, will help us to construct a complete picture of the effects of restriction of dynamical reactive processes on low-dimensional supports. In this respect, the case of complex oscillations and chaos is of special interest.

ACKNOWLEDGMENTS

The authors would like to thank Dr. G. Kalosakas for helpful discussions and Professor G. Nicolis for valuable ideas and for a critical reading of the manuscript. One of us, A.S., acknowledges financial support from the NATO Science Program. This work was supported, in part, by NATO Collaborative Research Grant No. CGR 973016, by the Belgian Federal Office for Scientific, Technical and Cultural Affairs within the framework of the ''Pôles d' Attractions Interuniversitaires'' program, and by the European Commission DG12 Grant No. PSS*1045.

[1] A. Harrison, *Fractals in Chemistry*, Oxford Chemistry Primers Vol. 22 (Oxford Science, Oxford, 1995).

[2] A.S. Mikhailov and A.Y. Loskutov, *Foundations of Synergetics* (Springer, New York, 1996).

[3] *Nonequilibrium Statistical Mechanics in One Dimension*, edited by V. Privman (Cambridge University Press, Cambridge, 1997).

[4] R.M. Ziff, E. Gulari, and Y. Barshad, Phys. Rev. Lett. **56**, 2553 (1986).

[5] B.J. Brosilow, E. Gulari, and R.M. Ziff, J. Chem. Phys. **98**, 674

(1993); C.A. Voigt and R.M. Ziff, Phys. Rev. E **56**, R6241 (1997).
[6] E.V. Albano and J. Marro, J. Chem. Phys. **113**, 10279 (2000).
[7] P. Meakin, J. Chem. Phys. **93**, 2903 (1991).
[8] J.W. Evans and M.S. Miesch, Phys. Rev. Lett. **66**, 833 (1991); M. Tammaro and J.W. Evans, Phys. Rev. E **52**, 2310 (1995); J. Chem. Phys. **104**, 3386 (1996); **108**, 762 (1998).
[9] D.J. Liu and J.W. Evans, Phys. Rev. Lett. **84**, 955 (2000).
[10] V.P. Zhdanov, Phys. Rev. E **59**, 6292 (1999); Surf. Sci. **426**, 345 (1999).
[11] H. Rose, H. Hempel, and L. Schimanksy-Geier, Physica A **206**, 421 (1994).
[12] V.P. Zhdanov, Phys. Rev. E **60**, 7554 (1995).
[13] H. Persson, P. Thormwälen, V.P. Zhdanov, and B. Kasemo, Catal. Today **53**, 273 (1999).
[14] G. Ertl, P.R. Norton, and J. Rustig, Phys. Rev. Lett. **49**, 177 (1982).
[15] M. Ehsasi, M. Matloch, O. Frank, J.H. Block, K. Christmann, F.S. Rys, and W. Hirschwald, J. Chem. Phys. **91**, 4949 (1989).
[16] R. Imbihl and G. Ertl, Chem. Rev. **95**, 697 (1995).
[17] Yu. Suchorski, J. Beben, E.W. James, J.W. Evans, and R. Imbihl, Phys. Rev. Lett. **82**, 1907 (1999); Yu. Suchorski, J. Beben, and R. Imbihl, Surf. Sci. **331**, 454 (2000).
[18] J. Wintterlin, S. Völkening, T.V.W. Janssens, T. Zambelli, and G. Ertl, Science **278**, 1931 (1997); S. Völkening and J. Wintterlin, J. Chem. Phys. **114**, 6382 (2001).
[19] A. Provata, J.W. Turner, and G. Nicolis, J. Stat. Phys. **70**, 1195 (1993).
[20] A. Tretyakov, A. Provata, and G. Nicolis, J. Phys. Chem. **99**, 2770 (1995).
[21] S. Prakash and G. Nicolis, J. Stat. Phys. **82**, 297 (1996).
[22] S. Prakash and G. Nicolis, J. Stat. Phys. **86**, 1289 (1997).
[23] J. Dethier, F. Baras, and M. Malek Mansour, Europhys. Lett. **42**, 19 (1998).
[24] M. Malek Mansour, J. Dethier, and F. Baras, J. Chem. Phys. **114**, 9265 (2001).
[25] A. Provata, G. Nicolis, and F. Baras, J. Chem. Phys. **110**, 8361 (1999).
[26] L. Frachebourg, P.L. Krapivsky, and E. Ben-Naim, Phys. Rev. E **54**, 6186 (1996).
[27] G.A. Tsekouras and A. Provata, Phys. Rev. E **65**, 016204 (2002).
[28] R. Imbihl, T. Fink, and K. Krisher, J. Chem. Phys. **96**, 6236 (1992).
[29] S.Y. Shvartsman, E. Schutz, R. Imbihl, and I.G. Kevrekidis, Phys. Rev. Lett. **83**, 2857 (1999).
[30] C. Voss and N. Kruse, Ultramicroscopy **73**, 211 (1998).
[31] M. Slinko, T. Fink, T. Loher, H.H. Madden, S.J. Lombardo, R. Imbihl, and G. Ertl, Surf. Sci. **264**, 157 (1992).
[32] C.G. Takoudis, L.D. Schmidt, and R. Aris, Surf. Sci. **105**, 325 (1981).
[33] M.A. McKarnin, R. Aris, and L.D. Schmidt, Proc. R. Soc. London, Ser. A **415**, 363 (1988).